PAPER • OPEN ACCESS

Topological defects in weak perpendicular magnetic anisotropy NdCo honeycomb lattices

To cite this article: F Valdés-Bango *et al* 2018 *New J. Phys.* **20** 113007

New Journal of Physics
The open access journal at the forefront of physics

Deutsche Physikalische Gesellschaft DPG
IOP Institute of Physics

Published in partnership with: Deutsche Physikalische Gesellschaft and the Institute of Physics

OPEN ACCESS

RECEIVED
3 July 2018

REVISED
24 September 2018

ACCEPTED FOR PUBLICATION
16 October 2018

PUBLISHED
6 November 2018

PAPER

Topological defects in weak perpendicular magnetic anisotropy NdCo honeycomb lattices

F Valdés-Bango[1,2], M Vélez[1,2], L M Alvarez-Prado[1,2] and J I Martín[1,2,3]

[1] Dpto. Física, Fac. Ciencias, Universidad de Oviedo, c/Federico Garcia Lorca 18, E-33007 Oviedo, Spain
[2] Centro de Investigación en Nanomateriales y Nanotecnología—CINN (CSIC—Univ. de Oviedo), E-33940 El Entrego, Spain
[3] Author to whom any correspondence should be addressed.

E-mail: jmartin@uniovi.es

Keywords: magnetic topological defect, magnetic force microscopy, weak perpendicular anisotropy, magnetic nanostructure

Abstract

Domain configuration has been studied by magnetic force microscopy and micromagnetic simulations in NdCo honeycomb lattices in comparison with similar patterned structures made of polycrystalline Co. The change in material anisotropy from in-plane to weak perpendicular magnetic anisotropy (wPMA) modifies the basic domain structure and relevant topological defects in the magnetization in each case: from in-plane domains, vortices, antivortices and half vortices in Co lattices to parallel stripe patterns with dislocations in NdCo samples with large enough thickness. A characteristic feature of wPMA materials is the possibility to drive the system from in-plane to stripe pattern configuration playing with sample thickness (during growth) or with magnetic anisotropy (as a function of temperature). It has allowed us to observe complex magnetic textures within the stripe pattern of NdCo samples imprinted from previous magnetic vortex and antivortex states that nucleate within the honeycomb lattice during the early stages of deposition and, then, become frozen by local rotatable anisotropy as sample thickness increases.

1. Introduction

Topological defects are a key to understanding global properties in many different condensed matter systems with long range order: linear and point defects such as dislocations, disclinations, vortices or antivortices may appear in such different systems as ferroelectrics, nematics, superconductors or ferromagnetic materials [1–4]. Chiral exchange interactions in magnetism allow the nucleation of magnetic skyrmions in non-centrosymmetric materials [5, 6] and in magnetic multilayers [7–9]. These textures present an enhanced topological stability that makes them very suitable for magnetic recording applications and logic devices [10–12]. Individual magnetic textures such as artificial skyrmions and merons can also be nucleated via domain imprinting in exchange coupled multilayers playing with geometry, in-plane and out-of-plane anisotropy layers or antiferromagnetic couplings [13–19]. In the case of magnetic nanostructures with in-plane magnetic anisotropy, magnetic vortices and edge half vortices are the most relevant topological defects needed to understand magnetization reversal [20] in nanowires [21] and bifurcations [22]. Also, in films with ordered arrays of antidots [23] or honeycomb lattices [24], it has been shown that vortex wall propagation can be controlled through the configuration of edge half vortices.

Magnetic films with weak perpendicular magnetic anisotropy (wPMA), such as amorphous NdCo alloy layers, display an equilibrium domain structure consisting of parallel stripe domains for large enough thickness [25]: the magnetization performs a weak out-of-plane oscillation around the average in-plane magnetization direction (see sketch in figure 1(a)) resulting in a periodic stripe pattern. The most common topological defects in these systems are magnetic dislocations (see figure 1(b)). Each dislocation is composed of a stripe bifurcation next to a stripe end-point, i.e. it is a so-called disclination dipole [26, 27]. In continuous films, dislocations appear randomly depending on magnetic history but, in patterned samples, it is possible to nucleate them at predefined positions playing with thickness modulations in a certain range of in-plane magnetic fields [28]. Also, stripe pattern dislocations are the preferred loci for nucleation of non-collinear meron textures [29] and

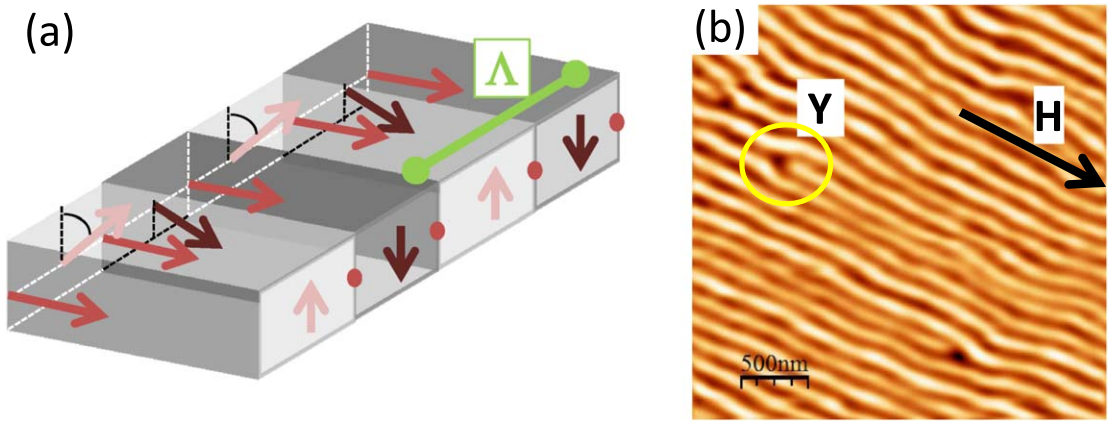

Figure 1. (a) Sketch of magnetization within stripe domain pattern. Λ indicates stripe pattern period. (b) MFM image of typical stripe domain pattern in continuous NdCo film at remanence. Y indicates a dislocation within the stripe pattern. Arrow marks the direction of the last applied field.

magnetic vortex–antivortex pairs during in-plane magnetization reversal [30]. Disorder in the system transforms the parallel stripe pattern into a labyrinth configuration, characterized by the dissociation of dislocations into free disclinations and the loss of orientational order [26, 27].

To move beyond dislocations and disclinations in wPMA materials, alternative strategies would be required, and they have only begun to be explored. This has been done, for example, by the application of out-of-plane magnetic fields in order to drive a transition from stripe pattern to dipolar skyrmion in amorphous Fe/Gd multilayers [31]. Other possibilities could be based in domain imprinting, as it is often done in multilayers that combine in-plane and out-of-plane anisotropy layers [16], or in geometrical confinement by sample patterning [32]. This last route has proved particularly interesting in the field of artificial spin ice systems [24, 33–35], in which the combination of confinement and frustration in complex geometries has been successfully used to nucleate high energy topological defects. For example, in honeycomb lattices made of in-plane magnetic anisotropy materials, such as permalloy or Co, complex combinations of transverse walls and magnetic half vortices have been observed at lattice nodes, stabilized by topological repulsion and global lattice disorder [35].

In this work, we have studied different processes for the nucleation of non-collinear magnetic textures in honeycomb lattices of NdCo alloys with wire width of the order of a few stripe domain periods, in comparison with in-plane anisotropy Co lattices of similar geometry. The presence of a wPMA anisotropy in the material implies additional ingredients that must be considered besides the usual shape anisotropy and Zeeman energy that govern magnetic nanostructures with in-plane anisotropy: (1) the relevant length scale in wPMA materials is determined by stripe domain period Λ, of the order of 100–200 nm depending on sample thickness [28]; (2) in-plane easy axis can be tuned by the last saturating field direction (i.e. they display rotatable magnetic anisotropy [36]); and (3) edge effects control magnetic stripe pattern orientation close to sample boundaries (i.e. energy is minimized for both normal and parallel orientation of stripe domains near the sample edge [37, 38]), as recently shown in NdCo samples patterned with hexagonal antidot arrays [39].

During isothermal magnetization reversal processes, rotatable anisotropy and edge effects dominate the magnetic behavior favoring parallel stripe patterns with a small amount of magnetic dislocations. A more interesting scenario appears when the samples are driven through the in-plane to stripe domain transition characteristic of wPMA materials when thickness increases above a critical value (t_c). This can be done either during sample growth (as grown state) or by thermal tuning of the magnetic anisotropy. Then, it is possible to observe complex non-collinear magnetic textures with in-plane configuration imprinted from in-plane magnetic vortices and antivortices with the addition of an out-of-plane oscillating component. These textures are configured by frustration and geometrical confinement when the system is in the low thickness or low anisotropy in-plane magnetization state. Then, as film thickness or out-of-plane anisotropy increase, local magnetization configuration of the magnetic texture is imprinted into the stripe pattern and stabilized by rotatable anisotropy resulting in the corresponding topological defect.

2. Experimental

Two series of analogous honeycomb arrays were fabricated either with Co (in-plane anisotropy) or NdCo (wPMA) in order to compare the effect of material anisotropy in samples with the same geometry and similar saturation magnetization M_S. Briefly, the desired arrays were fabricated by a combination of e-beam lithography and lift-off

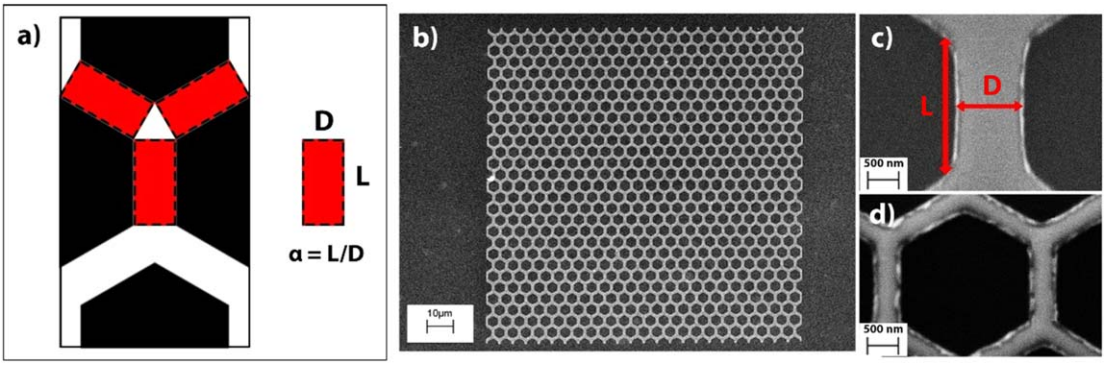

Figure 2. (a) Unit pattern of honeycomb lattice, periodically replicated by e-beam lithography on a 100 μm $\times$ 100 μm area. Sketch of vertical bar dimensions: width (D) and length (L). (b) Scanning electron microscopy (SEM) image of Co array with $D = 0.8$ μm $L = 2.1$ μm; (c) SEM image of a detail of the array in (b); (d) SEM image of a $NdCo_5$ array with $D = 0.4$ μm and $L = 1.2$ μm.

on Si(100) substrates as reported before [40]. Each honeycomb array is written by the periodic repetition of a simple unit cell (shown in figure 2(a)) over an area of 100 μm $\times$ 100 μm on a PMMA covered Si substrate. Basic array geometrical dimensions are given by bar width (D) and length (L), which are varied in the range 0.4–4 μm, with aspect ratio $\alpha = L/D$ in the range 1–4 in order to explore different regimes for the nucleation of magnetic textures in the system. Area size (100 μm $\times$ 100 μm) was chosen to include a large enough number of honeycomb unit cells to minimize border effects on collective dynamics in the spin ice regime [41]. Several arrays with different geometrical parameters are written in the same Si substrate, separated by 500 μm distance from their neighbors, in order to ensure reproducibility of the same magnetic history in the different arrays studied.

To prepare honeycomb lattices of magnetic material with in-plane magnetic anisotropy, a 40 nm Co layer was grown by sputtering on the lithographed samples. Then, the final Co nanostructures were obtained by lift-off in acetone, as shown in figures 2(b), (c). wPMA honeycomb lattices were fabricated with a similar procedure with the deposition of a 60 nm thick layer of $NdCo_5$ alloy from co-sputtering of two individual Nd and Co targets [28]. Sample thickness is chosen to be above the critical thickness for nucleation of stripe domains in this material, which is of the order of 45 nm at room temperature [42]. Sample was rotated continuously during the deposit in order to preclude in-plane anisotropies. A typical NdCo nanostructure is shown in figure 2(d).

The magnetic behavior of each honeycomb array was characterized by magnetic force microscopy (MFM) with a Nanotec™ atomic force microscope and Nanosensors™ PPP-MFMR cantilevers with spring constant 3 N m^{-1} [28]. MFM images were obtained using the dynamical retrace mode in which the magnetic signal is acquired in a retrace scan at a 50 nm lift height following the topography profile acquired previously. The arrays were always imaged at remanence, with different magnetic histories: as grown, in-plane magnetized with the field H parallel to one of the arrays bar axis (longitudinal configuration) or in-plane magnetized with the field H perpendicular to one of the arrays bar axis (transverse configuration). The maximum in-plane field in each magnetization process was 0.55 T.

MFM images were compared with micromagnetic simulations performed with the finite difference code MuMax^3 [43], with a discretization into cells of dimensions of 7 $\times$ 7 $\times$ 3 nm^3. MuView code was used for visualization. Material parameters for NdCo nanostructures at room temperature were $M_S = 10^6$ A m^{-1}, $A = 0.5 \times 10^{-11}$ J m^{-1}, $K_N = 10^5$ J m^{-3}, as reported before [19]. The lattice was simulated using periodic boundary conditions over space, so that the unit cells are repeated 20 $\times$ 15 times in the longitudinal and transverse directions, respectively. The size of the repeated unit blocks varied from a simple unit as in figure 2(a) to a set of 4 $\times$ 3 hexagonal cells. The simulations were also performed in the absence of periodic boundary conditions, with very similar qualitative results in the observed domain configurations and magnetic textures.

3. Results and discussion

3.1. Ordered states: parallel and transverse remanence

MFM images of the remanent configuration of Co honeycomb arrays are shown in figure 3 after saturating the sample either in the longitudinal (H parallel to bar axis) or transverse (H perpendicular to bar axis) direction. The longitudinal configuration corresponds to a magnetic easy axis and is shown in figure 3(a). Bar intersections appear as white (or black) contrast triangular regions. This image is consistent with a pseudo spin ice configuration in which each bar is in a single dipole state [33, 34] with the magnetization parallel to the bar axis and orientation closest to the applied field direction [33]. As sketched by thin arrows in figures 3(a), (b), a white

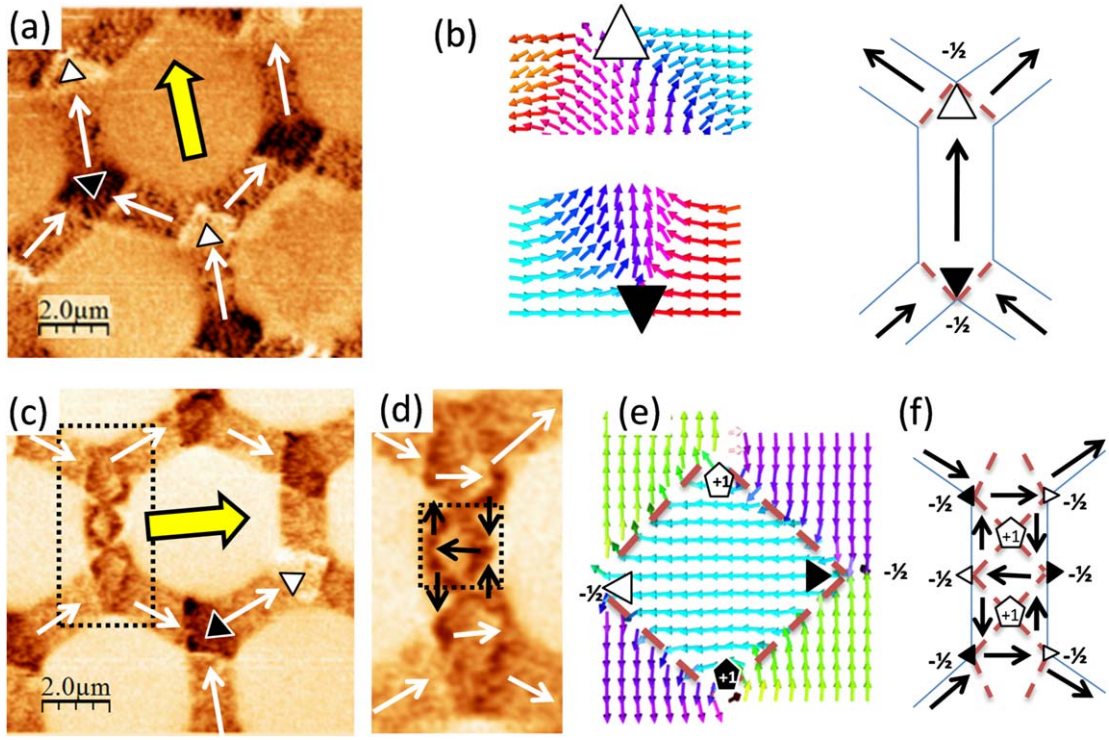

Figure 3. Magnetization configuration of Co honeycomb array at remanence after longitudinal and transverse saturation ($D = 1$ μm, $L = 2$ μm): (a) MFM image at longitudinal remanence; (b) sketch of magnetization configuration around $-1/2$ edge half vortices (indicated as triangles) and their location at the honeycomb lattice intersections in the longitudinal remanence state; (c) MFM image of transverse remanence; (d) zoom of dotted region in (c) showing a detail of magnetic configuration in a transverse bar; (e) micromagnetic simulation of Co bar with transverse magnetization (equivalent to square dotted region in (d)): a 'square unit' is formed made up of two vortices of opposite chirality (marked by small pentagons) and two edge half vortices (marked by small triangles) linked by 90° domain walls (marked by dashed lines). Note that the different shapes used to mark topological defects are guides to the eye, unrelated to the symmetry of the magnetic textures; (f) sketch of magnetization configuration and topological defects in (d) with two vortices at the bar center and six half vortices at domain wall intersections at the bar edge.

(black) intersection corresponds to a 1-in/2-out (or 2-in/1-out) configuration. The detailed micromagnetic configuration at each intersection is governed by the need to minimize magnetostatic energy with the magnetization parallel to sample boundaries [20]. Singular points appear whenever the local magnetization meets head to head (or tail to tail) along the border. These points are the nuclei of edge half vortices as defined by Tchernyshyov and Chern [20] (see triangles in figure 3(b)) with fractional topological index $-1/2$ calculated from the rotation of the magnetization at the sample boundary [20, 24]. At longitudinal remanence, white/black contrast regions are arranged in interleaving hexagonal lattices and there is a pair of edge half vortices at each hexagonal hole of the honeycomb lattice [24], indicated by black/white triangles in figures 3(a), (b). They are located at opposite hole sides, determined by the orientation of the average remanent magnetization.

The transverse remanence state is shown in figure 3(c) and corresponds to a magnetic hard axis of the honeycomb array. In this case, bars closest to the saturating field orientation keep the single dipole character (see thin arrows in figure 3(c)) organized in zig–zag chains that oscillate around the transverse direction. However, bars transverse to the saturating field may break up into domains (see dotted rectangle in figure 3(c)) creating complex multidomain structures. Their role is to resolve magnetic frustration between chains without raising magnetostatic energy. They are composed of 'square units' made of vortices of alternating chirality at the bar center and half vortices at the edge (see figures 3(d)–(f)). Vortices and half vortices are linked by 90° walls, i.e. domain walls in which the magnetization rotates by 90° (marked by dashed lines in figure 3(e)). This configuration minimizes magnetostatic energy and is characterized by the presence of small transverse domains with rhomboid shape (see figure 3(e)).

The number of units that fit in a given bar is a function of its geometrical dimensions D and L. As the aspect ratio increases, a larger number of these 'square units' will fit in a transverse bar. It is interesting to note that the total winding number (as defined in [20]) of the 'square unit' shown in figure 3(e) is zero. It is made of two half vortices with w(edge half vortex) $= -1/2$, and one vortex with w(vortex) $= 1$ (since the two vortices shown in figure 3(e) are shared between neighboring units), so that w(square unit) $= 1 + 2 \times (-1/2) = 0$. Thus, the total winding number of the transverse bar is always the same, independently of the number of domains, just fixed by the boundary conditions of parallel magnetization at both ends of the bar (i.e. a total 360° rotation). For

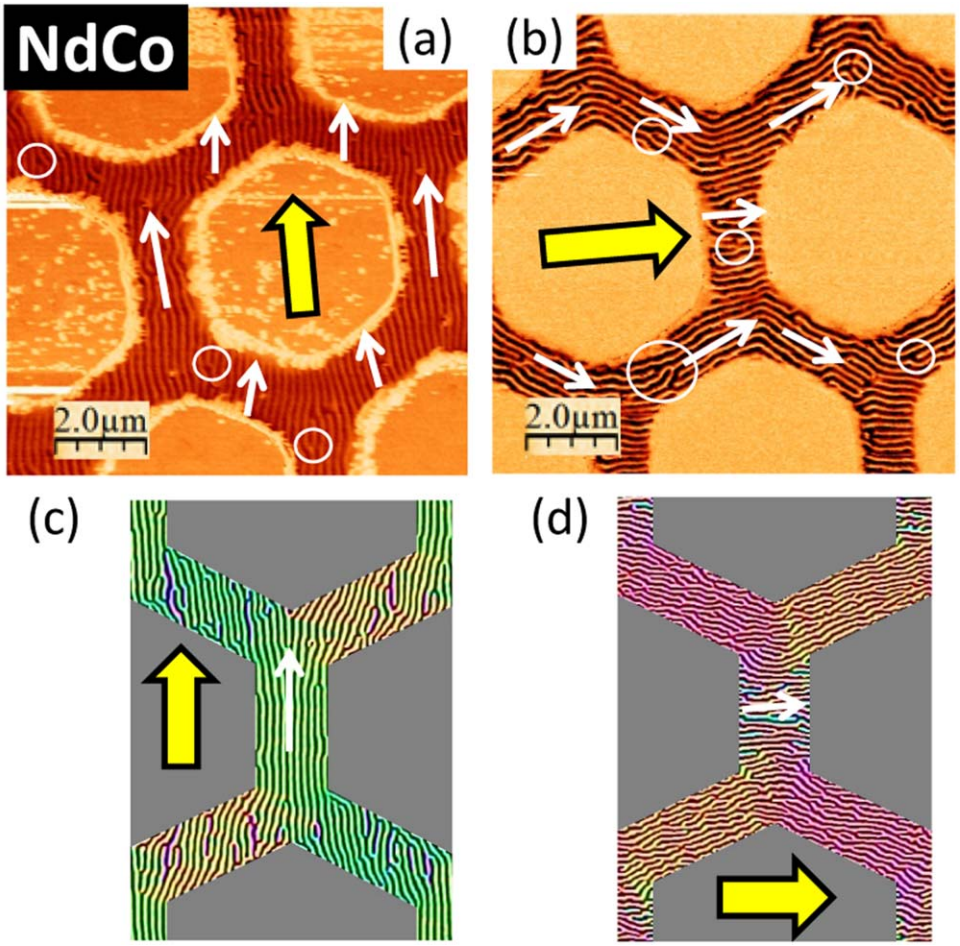

Figure 4. Magnetic configuration of NdCo honeycomb arrays at remanence after longitudinal and transverse saturation ($D = 1$ μm, $L = 2$ μm) with stripe pattern of period $\Lambda = 150$–160 nm: (a) MFM image at longitudinal remanence, (b) MFM image at transverse remanence; micromagnetic simulation of NdCo array at (c) longitudinal and (d) transverse remanence. Circles in (b) mark the position of some dislocations within the stripe domain pattern. Thin arrows indicate local magnetization orientation and thick arrows last saturating field direction.

example, in the domain structure shown in figure 3(f) there are two vortices and six half vortices, so the total winding number is $w = 2 \times 1 + 6 \times (-1/2) = -1$. This is the same winding number as the single domain bars with two edge half vortices shown in figure 3(b) ($w = 2 \times (-1/2) = -1$), making both structures topologically equivalent. These multidomain structures were also observed in other Co honeycomb arrays with dimensions ($D = 1.5$ μm, $L = 4.5$ μm), ($D = 2.2$ μm, $L = 4.3$ μm) and ($D = 1.3$ μm, $L = 2.3$ μm). In all the cases, the total winding number was the same ($w = -1$), but with a different number of rhomboid units depending on bar length and aspect ratio. It must be noted that, in this range of array geometrical parameters, multidomain structures are the most common magnetic configuration for transverse bars at the transverse remanent state (between 50% and 90% of cases).

For a $NdCo_5$ honeycomb lattice with similar geometrical dimensions (figure 4), MFM images reveal a magnetic configuration composed of parallel stripe domains. Stripe pattern period is $\Lambda = 180$ nm, which is comparable to 1 μm bar width (about 5 to 6 stripe periods fit within each bar). The observed behavior is quite different from Co arrays: both in the longitudinal and transverse remanent states the stripe pattern is mainly aligned along the last saturating field direction, in agreement with micromagnetic simulations (figures 4(c), (d)). One of the reasons for these differences is rotatable anisotropy in wPMA materials [36] that creates a field-dependent strong easy-axis and favors magnetization orientation along the last saturation field. The second one is related to edge effects of the stripe domain pattern. Energy can be minimized both for parallel and perpendicular stripe orientation at the sample edge [37]. Then, taking into account that the average in plane magnetization component of the stripe pattern is always along the stripes (figure 1(a)), both factors contribute to the observed configuration. At remanence, stripes and magnetization are, on average, aligned along the last saturation field. They only turn slightly at sample edges to meet them either parallel or transverse (approximately in a 400 nm range from edge). A consequence of the more homogenous in-plane magnetization orientation is that the typical vortex/half vortex configurations of the Co honeycomb arrays disappear and local

magnetization deviations are resolved with the nucleation of dislocations within the periodic stripe pattern (see circles in figures 4(a), (b)).

3.2. Disordered states: as-grown remanence

A traditional technique to explore disordered structures in artificial spin ice systems with in-plane magnetization is to study samples in as-grown configuration [44–46]. The smaller thickness of the sample during the fabrication process allows the system to explore a different energy region (with higher effective temperature) that becomes frozen as sample thickness increases. This enhanced disorder clearly shows up in the MFM images of Co and NdCo honeycomb arrays in the as grown state (figure 5). In cobalt arrays, multidomain behavior is obtained again (see figures 5(a), (b)) very similar to the transverse remanence images in figure 3(c). We observe a mixture of double-vortex bars equivalent to the configuration in figure 3(d) (indicated by pairs of pentagons in figures 5(f), (g)), vortex–antivortex bars (indicated by a square and a pentagon at the left of figure 5(f)) and single domain bars bounded by pairs of half vortices indicated as triangles in figure 5(g). In the multidomain bars, additional half vortices appear at the sample edges (not indicated in figures 5(f), (g) for clarity), so that the total winding number of each bar is kept constant at $w = -1$.

In the as-grown $NdCo_5$ arrays (figures 5(c)–(e)), the magnetic configuration is much richer than in the transverse and longitudinal remanence states with non-trivial magnetic structures, such as concentric circles, spiral stripes, free bifurcations and end-points or sharp stripe turns (some of these structures are highlighted in figures 5(h)–(j)). These curved domain patterns can be understood as contour lines for the in-plane magnetization configuration in the system [26].

This is a consequence of the Bloch character of domain walls that separate up/down stripe domains (i.e. in-plane magnetization is tangent to the lines that separate black/white stripes in the MFM images). Then, the set of concentric circles marked by pentagons in figure 5, could correspond to the contour lines of an in-plane vortex (similar to those found in the Co honeycomb arrays) but with the addition of an out-of-plane component due to the presence of the magnetic stripe pattern. Then, the black (or white) circular domains at the 'vortex core' should be skyrmion-like textures composed of an in-plane vortex and an out-of-plane polarity change. Two skyrmion-like textures can be seen inside the vertical bar in figure 5(c) (marked by two pentagons in figure 5(h)). This pair of textures resembles the double-vortex structure sketched in figure 3(d) (and also observed in figures 5(a), (b)) as they share a very similar in-plane magnetization configuration made of two neighboring rotating regions. The main differences appear in the bar section in between the two vortices (or the two skyrmion-like objects): instead of the transverse rhomboid domains typical of Co samples, the two sets of concentric circles in the NdCo image are separated by a set of parallel stripes transverse to bar width. This can be attributed to the different boundary conditions for in-plane and wPMA materials: edge half vortices appear in Co bars to force a parallel magnetization configuration along sample borders; however, in wPMA NdCo energy can also be minimized with a stripe pattern normal to sample edge.

In the upper part of the bar, a single bifurcation of a white stripe is observed (marked by a triangle in figure 5(h)). In the classification of topological defects within the stripe pattern [26], a free bifurcation (or a free stripe end-point) corresponds to a defect with a fractional topological number, so called −½ disclination (or $+1/2$ disclination). A dislocation within the stripe pattern is composed of a bifurcation bounded to a stripe end-point (i.e. a disclination dipole), resulting in a defect with an integer topological index (Burgers vector given by the stripe pattern period) [26]. In wPMA materials, free disclinations are not confined to sample boundaries in spite of their fractional topological index (in contrast with half vortices in the Co honeycomb arrays) and their presence is associated with the loss of long range orientational order within the stripe pattern and the transition to a labyrinth configuration [26]. Pairs of triangles at the bottom of figure 5(i) and at the right of figure 5(j) correspond to dissociated disclination dipoles. These high energy configurations usually appear in the stripe pattern to accommodate strong deviations from the parallel uniform state, and they are observed here at high curvature regions of the stripe pattern. At some bar intersections we also observe 'undulation instabilities' of the stripe pattern [27], marked as dashed lines in figure 5, that appear related with in-plane domain walls as observed in the Co honeycomb arrays. More complex defects appear in the system by non-standard combinations of ½ disclinations: stripe spirals, marked by rhombs in figures 5(i), (j), are a combination of a black and a white end-points (two $+1/2$ disclinations) that rotate around each other; and a stripe saddle point can be seen in figures 5(e) and (j), marked by a square, which is a combination of two black bifurcations (two $-1/2$ disclinations).

3.3. Thermal imprinting of complex topological defects: micromagnetic simulations

It is reasonable to think that the complex domain configurations observed in the as-grown states of figure 5 are formed in the early stages of deposition with small film thickness and, then, they become frozen as film thickness increases. Particularly, in the case of wPMA materials, film thickness t plays an important role in the interplay

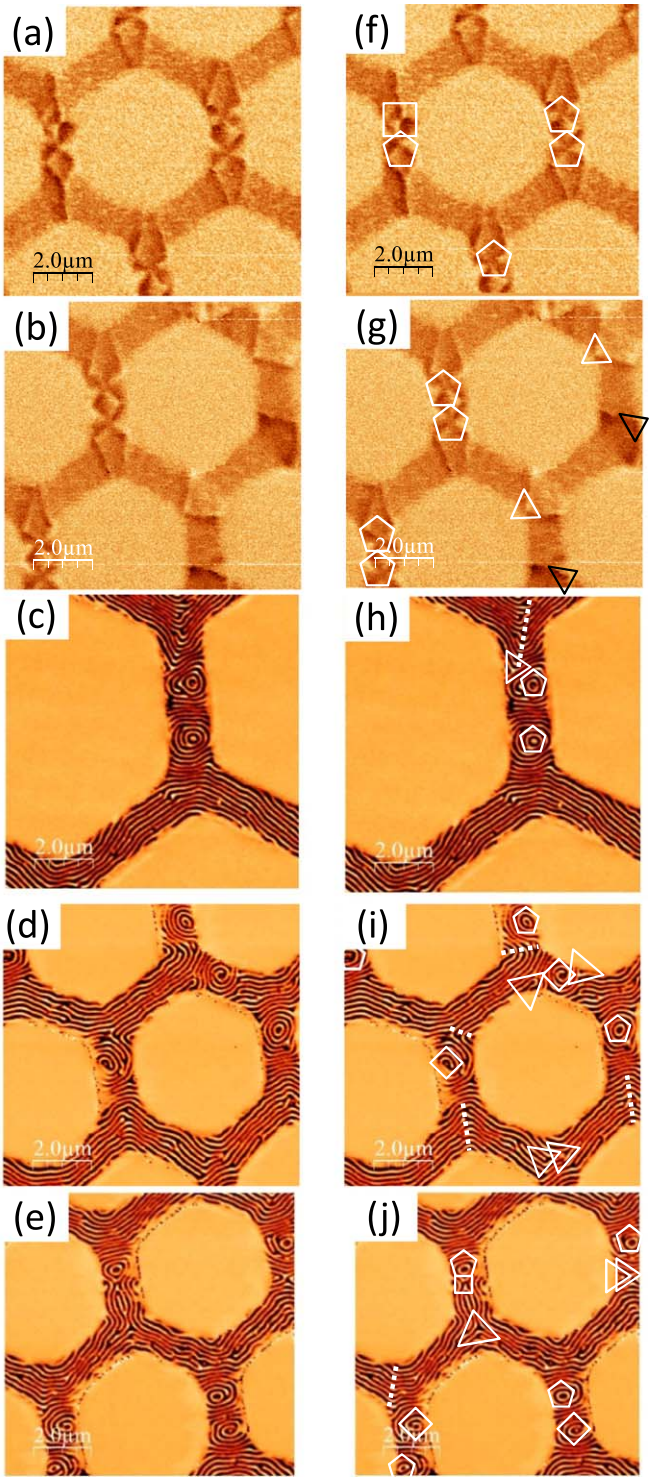

Figure 5. MFM images of honeycomb arrays in as-grown configuration (1 μm bar width): (a), (b) Cobalt arrays exhibiting multidomain structures and (c)–(e) $NdCo_5$ arrays with analogous configurations; (f)–(j) are the same images with topological defects indicated as pentagons (vortices), squares (antivortices), ½ disclinations (triangles) and spirals (rhombs). Dashed lines indicate 'undulation' instabilities of the stripe pattern. Note that the different shapes used to mark topological defects are guides to the eye, unrelated to the symmetry of the magnetic textures.

between magnetostatic energy $\frac{1}{2}\mu_0 M_S^2$ and out-of-plane anisotropy K_N: for t below a critical thickness t_c, magnetostatic energy dominates and the magnetic behavior is equivalent to in-plane anisotropy materials [25] whereas the stripe pattern only nucleates for $t > t_c$. In general, t_c depends on the ratio of $K_N/\frac{1}{2}\mu_0 M_S^2$ [25], which is strongly temperature dependent in NdCo alloys [47, 48]. Then, a possible route to drive the transition from in-plane to stripe pattern configuration is to increase film thickness at constant temperature (i.e. during sample growth). Another possibility, once that the film has been grown, would be to reduce the measurement temperature at constant thickness in order to decrease t_c below t. For $NdCo_5$ alloys, a 30 K temperature decrease

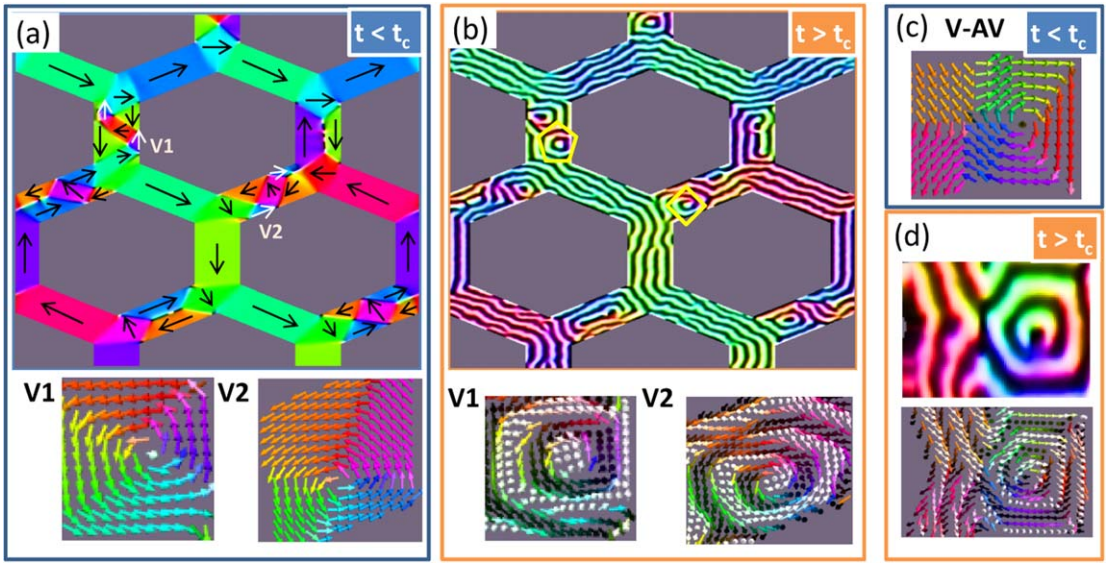

Figure 6. Micromagnetic simulations of disordered states in the same honeycomb array with different K_N: (a) vortex states with in-plane magnetization: $K_N = 10^4$ J m^{-3} and $t < t_c$; (b) equivalent pattern to (a) with weak stripe pattern: $K_N = 10^5$ J m^{-3} and $t > t_c$. Bottom panels are details of the micromagnetic spin configuration in V1 and V2 in the low and high K_N states. (c) Vortex–antivortex pair with $t < t_c$. (d) Equivalent spin configuration to (c) for $t > t_c$.

from 330 to 300 K implies an order of magnitude increase in K_N [47], which should be enough to change the magnetic behavior from in-plane to stripe pattern in the 60 nm thick films considered in this work.

In order to test this hypothesis, we have performed a set of micromagnetic simulations in 60 nm thick honeycomb arrays with varying K_N to drive the transition from in-plane magnetization to stripe pattern configuration. For each array a similar procedure was carried out: starting from a random seed, we let the system achieve equilibrium with a high $K_N = 10^5$ J m^{-3}; then, K_N is reduced in one order of magnitude and energy is minimized again (which would be equivalent to heating the samples 30 K above room temperature). Figure 6(a) shows a typical magnetization configuration obtained in this low K_N state, which is very similar to the experimental configuration observed in as-grown Co arrays: several bars are broken in multidomain states with different combinations of in-plane vortices and half vortices (the detailed spin configuration of two vortices, labelled as V1 and V2 is displayed at the lower part of figure 6(a)). Then, taking this low K_N micromagnetic configuration as a starting point, out-of-plane anisotropy is increased to its room temperature value (so that t_c decreases below film thickness) and the minimum energy domain configuration is calculated again. The result of this procedure is shown in figure 5(b): the honeycomb array displays a stripe pattern that follows the local in-plane magnetic orientations given by the previous low K_N domain structure, very similar to the as grown stripe patterns observed in figure 5, indicating that rotatable anisotropy has acted on a local scale to 'freeze' in-plane domains and translate them into the stripe domain configuration.

The addition of the out-of-plane oscillating magnetization of the stripe pattern transforms in plane magnetic vortices into different kinds of skyrmion-like bubbles. For example, vortex V1 in figure 6(a) gives rise to a small circular bubble inside a set of concentric stripes in figure 6(b): at the center we find a small texture with the same in-plane chirality as V1, but with a full rotation in the out-of-plane magnetization component from $+M_z$ to $-M_z$ (i.e. with a skyrmion like configuration) and size given by the lateral stripe pattern periodicity (see details marked by hollow pentagons in figures 6(b) and 5(h)–(j)). Vortex V2 shows a different transformation path that leads into a stripe domain spiral (see rhomb in figure 6(b)) with rotation sense given by the original in-plane vortex chirality. At the spiral center, the rotating white stripe is pinched resulting in a partially detached bubble. Pinching of a stripe end-point has been shown to create skyrmion bubbles in trilayers [9] and, recently, Garanin *et al* [49] have shown that, in centrosymmetric crystals, skyrmion-like objects can detach from stripe domains aided by Bloch lines inside domain walls. Thus, this could be the origin of the small circular domains observed inside some of the spiral stripes of figures 5(i), (j).

The skyrmionic numbers Q (as defined in [49, 50]) of the observed textures have been estimated from the micromagnetic simulations. At the low K_N state depicted in figure 5(a), Q is in the range $Q \approx 0.4$–0.5 for V1 and V2, as expected for magnetic vortices [49]. At the high K_N state depicted in figure 5(b), skyrmionic numbers increase up to $Q \approx 0.8$–0.9 due to the enhancement of out-of-plane magnetization components, confirming their skyrmion-like character.

Finally, figures 6(d), (e) show the transformation of an in-plane vortex–antivortex pair for $t < t_c$ into texture that resembles a coupled skyrmion–antiskyrmion pair for $t > t_c$. The antivortex in-plane magnetization saddle point guides the nucleation of a double bifurcation in a dark stripe with skyrmionic number $Q \approx -0.8$. Next to it there is a set of concentric circular stripes derived from the in-plane magnetic vortex. At the center, we find a partially detached circular bubble with positive skyrmionic number $Q \approx 0.6$. This results in a very similar stripe configuration to the one marked by the pentagon-square pair in figure 5(j).

4. Conclusions

In summary, the magnetic configuration of honeycomb arrays has been characterized by MFM, comparing the configurations of samples either with in-plane magnetic anisotropy (Co) or wPMA (NdCo) with similar geometrical dimensions and magnetic history. Ordered states appear after longitudinal and transverse remanence characterized by a combination of single domain and multidomain bars in the Co arrays and by parallel stripe patterns with dislocations in NdCo arrays. On the other hand, disordered states are found in as grown arrays: in the case of Co patterned samples, we observe multidomain structures that can be understood in terms of simple topological defects such as vortices, antivortices and half vortices; in the wPMA NdCo arrays, a variety of skyrmion-like stripe configurations are found (concentric circles, spirals, bifurcations); they are closely related with in-plane vortices and antivortices with an additional oscillating out-of-plane magnetization component. The comparison between the experimental MFM images and micromagnetic simulations shows that the transition from in-plane magnetization to stripe domain structure in NdCo films (driven either by thickness increase during deposition or by the temperature dependence of K_N) is at the origin of the observed stripe configurations. It opens a route to nucleate tailored magnetic textures in wPMA materials starting from in-plane multidomain states in a two-step process: first, an in-plane magnetic configuration is designed by geometrical confinement and/or magnetic history when the sample is in a low K_N state (i.e. with parallel boundary conditions for the magnetization); then, K_N is increased (by reducing temperature) in order to transfer it to the stripe domain pattern as it nucleates in the film. The result would be a tuned non-collinear magnetic texture with enhanced skyrmionic number due to the addition of out-of-plane magnetization components.

Acknowledgments

Work supported by Spanish MINECO (grant FIS2016-76058 (AEI/FEDER,EU) 'Una manera de hacer Europa').

ORCID iDs

M Vélez https://orcid.org/0000-0003-0311-7434
L M Alvarez-Prado https://orcid.org/0000-0002-3890-4983
J I Martín https://orcid.org/0000-0003-2256-0909

References

[1] Prokhorenko S, Nahas Y and Bellaiche L 2017 Fluctuations and topological defects in proper ferroelectric crystals *Phys. Rev. Lett.* **118** 147601
[2] Alexander G P, Chen B G, Matsumoto E A and Kamien R D 2012 Colloquium: disclination loops, point defects, and all that in nematic liquid crystals *Rev. Mod. Phys.* **84** 497
[3] Nagaosa N and Tokura Y 2013 Topological properties and dynamics of magnetic skyrmions *Nat. Nanotechnol.* **8** 899
[4] Gingras M J P and Huse D A 1996 Topological defects in the random-field XY model and the pinned vortex lattice to vortex glass transition in type-II superconductors *Phys. Rev.* B **53** 15193
[5] Rossler U K, Bogdanov A N and Pfleiderer C 2006 Spontaneous skyrmion ground states in magnetic metals *Nature* **442** 797
[6] Yua X, Mostovoy M, Tokunaga Y, Zhang W, Kimoto K, Matsui Y, Kaneko Y, Nagaosa N and Tokura Y 2012 Magnetic stripes and skyrmions with helicity reversals *Proc. Natl Acad. Sci.* **109** 8856
[7] Porter N A, Spencer C S, Temple R C, Kinane C J, Charlton T R, Langridge S and Marrows C H 2015 Manipulation of the spin helix in FeGe thin films and FeGe/Fe multilayers *Phys. Rev.* B **92** 144402
[8] Moreau-Luchaire C *et al* 2016 Additive interfacial chiral interaction in multilayers for stabilization of small individual skyrmions at room temperature *Nat. Nanotechnol.* **11** 444
[9] Jiang W *et al* 2015 Blowing magnetic skyrmion bubbles *Science* **349** 283
[10] Tomasello R, Martinez E, Zivieri R, Torres L, Carpentieri M and Finocchio G 2014 A strategy for the design of skyrmion racetrack memories *Sci. Rep.* **4** 6784
[11] Zhang X, Ezawa M and Zhou Y 2015 Magnetic skyrmion logic gates: conversion, duplication and merging of skyrmions *Sci. Rep.* **5** 9400
[12] Zhou Y and Ezawa M 2014 A reversible conversion between a skyrmion and a domain-wall pair in a junction geometry *Nat. Commun.* **5** 4652
[13] Streubel R *et al* 2015 Manipulating topological states by imprinting non-collinear spin textures *Sci. Rep.* **5** 8787

[14] Miao B F et al 2014 Experimental realization of two-dimensional artificial skyrmion crystals at room temperature Phys. Rev. B 90 174411
[15] Dai Y Y, Wang H, Tao P, Yang T, Ren W J and Zhang Z D 2013 Skyrmion ground state and gyration of skyrmions in magnetic nanodisks without the Dzyaloshinsky–Moriya interaction Phys. Rev. B 88 054403
[16] Gilbert D, Maranville B B, Balk A L, Kirby B J, Fischer P, Pierce D T, Unguris J, Borchers J A and Liu K 2015 Realization of ground-state artificial skyrmion lattices at room temperature Nat. Commun. 6 8462
[17] Zhou Y, Iacocca E, Awad A A, Dumas R K, Zhang F C, Braun H B and Åkerman J 2015 Dynamically stabilized magnetic skyrmions Nat. Commun. 6 8193
[18] Senthil T, Vishwanath A, Balents L, Sachdev S and Fisher M P A 2004 Deconfined quantum critical points Science 303 1490
[19] Hierro-Rodriguez A, Quirós C, Sorrentino A, Blanco-Roldán C, Alvarez-Prado L M, Martín J I, Alameda J M, Pereiro E, Vélez M and Ferrer S 2017 Observation of asymmetric distributions of magnetic singularities across magnetic multilayers Phys. Rev. B 95 014430
[20] Tchernyshyov O and Chern G W 2005 Fractional vortices and composite domain walls in flat nanomagnets Phys. Rev. Lett. 95 197204
[21] Thomas L, Hayashi M, Moriya R, Rettner C and Parkin S 2012 Topological repulsion between domain walls in magnetic nanowires leading to the formation of bound states Nat. Commun. 3 810
[22] Sethi P, Murapaka C, Goolaup S, Chen Y J, Leong S H and Lew W S 2016 Direct observation of deterministic domain wall trajectory in magnetic network structures Sci. Rep. 6 19027
[23] Herrero-Albillos J et al 2018 2D magnetic domain wall ratchet: the limit of submicrometric holes Mater. Des. 138 111
[24] Pushp A, Phung T, Rettner C, Hughes B P, Yang S-H, Thomas L and Parkin S S P 2013 Domain wall trajectory determined by its fractional topological edge defects Nat. Phys. 9 505
[25] Hubert A and Schäfer R 1998 Magnetic Domains: The Analysis of Magnetic Nanostructures (Berlin: Springer)
[26] Seul M and Andelman D 1995 Domain shapes and patterns: the phenomenology of modulated phases Science 267 476–83
[27] Seul M and Wolfe R 1992 Evolution of disorder in magnetic stripe domains: I. Transverse instabilities and disclination unbinding in lamellar patterns Phys. Rev. A 46 7519
[28] Hierro-Rodriguez A, Cid R, Vélez M, Rodriguez-Rodriguez G, Martín J I, Alvarez- Prado L M and Alameda J M 2012 Topological defects and misfit strain in magnetic stripe domains of lateral multilayers with perpendicular magnetic anisotropy Phys. Rev. Lett. 109 117202
[29] Blanco-Roldán C et al 2015 Nanoscale imaging of buried topological defects with quantitative x-ray magnetic microscopy Nat. Commun. 6 8196
[30] Hierro-Rodriguez A et al 2017 Deterministic propagation of vortex–antivortex pairs in magnetic trilayers Appl. Phys. Lett. 110 262402
[31] Montoya S A et al 2017 Tailoring magnetic energies to form dipole skyrmions and skyrmion lattices Phys. Rev. B 95 024415
[32] Zhang S S L, Phatak C, Petford-Long A K and Heinonen O G 2017 Tailoring magnetic skyrmions by geometric confinement of magnetic structures Appl. Phys. Lett. 111 242405
[33] Ladak S, Read D E, Perkins G K, Cohen L F and Branford W R 2010 Direct observation of magnetic monopole defects in an artificial spin-ice system Nat. Phys. 6 359
[34] Qi Y, Brintlinger T and Cumings J 2008 Direct observation of the ice rule in an artificial kagome spin ice Phys. Rev. B 77 094418
[35] Zeissler K, Chadha M, Lovell E, Cohen L F and Branford W R 2016 Low temperature and high field regimes of connected kagome artificial spin ice: the role of domain wall topology Sci. Rep. 6 30218
[36] Hierro-Rodriguez A, Vélez M, Morales R, Soriano N, Rodríguez-Rodríguez G, Álvarez-Prado L M, Martín J I and Alameda J M 2013 Controlled nucleation of topological defects in the stripe domain patterns of lateral multilayers with perpendicular magnetic anisotropy Phys. Rev. B 88 174411
[37] Clarke D, Tretiakov O A and Tchernyshyov O 2007 Stripes in thin ferromagnetic films with out-of-plane anisotropy Phys. Rev. B 75 174433
[38] Lee S H, Zhu F Q, Chien C L and Marković N 2008 Effect of geometry on magnetic domain structure in Ni wires with perpendicular anisotropy: a magnetic force microscopy study Phys. Rev. B 77 132408
[39] Valdes-Bango F, Vélez M, Alvarez-Prado L M, Alameda J M and Martín J I 2017 Magnetic stripes and holes: complex domain patterns in perforated films with weak perpendicular anisotropy AIP Adv. 7 056303
[40] Martín J I, Vélez M, Alameda J M, Briones F and Vicent J L 2002 Fabrication and magnetic properties of arrays of amorphous and polycrystalline ferromagnetic nanowires obtained by electron beam lithography J. Magn. Magn. Mater. 240 14
[41] Mengotti E, Heyderman L J, Fraile Rodríguez A, Bisig A, Le Guyader L, Nolting F and Braun H B 2008 Building blocks of an artificial kagome spin ice: photoemission electron microscopy of arrays of ferromagnetic islands Phys. Rev. B 78 144402
[42] Valdés-Bango F et al 2012 Perpendicular magnetic anisotropy in Nd-Co alloy films nanostructured by di-block copolymer templates J. Appl. Phys. 112 083914
[43] Vansteenkiste A, Leliaert J, Dvornik M, Helsen M, Garcia-Sanchez F and Van Waeyenberge B 2014 The design and verification of MuMax3 AIP Adv. 4 107133
[44] Nisoli C, Moessner R and Schiffer P 2013 Colloquium: artificial spin ice: designing and imaging magnetic frustration Rev. Mod. Phys. 85 1473
[45] Rodrigues J H, Mól L A S, Moura-Melo W A and Pereira A R 2013 Efficient demagnetization protocol for the artificial triangular spin ice Appl. Phys. Lett. 103 092403
[46] Porro J M, Bedoya-Pinto A, Berger A and Vavassori P 2013 Exploring thermally induced states in square artificial spin-ice arrays New J. Phys. 15 055012
[47] Cid R, Rodríguez-Rodríguez G, Álvarez-Prado L M, Díaz J and Alameda J M 2007 Temperature dependence of the anisotropy of amorphous NdCo5 thin films J. Magn. Magn. Mater. 316 e446
[48] Alvarez-Prado L M, Cid R, Morales R, Diaz J, Vélez M, Rubio H, Hierro-Rodriguez A and Alameda J M 2018 Determination of the out-of-plane anisotropy contributions (first and second anisotropy terms) in amorphous Nd-Co thin films by micromagnetic numerical simulations J. Magn. Magn. Mater. 456 251
[49] Garanin D A, Chudnovsky E M and Zhang X 2017 Skyrmion clusters from Bloch lines in ferromagnetic films Europhys. Lett. 120 17005
[50] Heinze S, von Bergmann K, Menzel M, Brede J, Kubetzka A, Wiesendanger R, Bihlmayer G and Blügel S 2011 Spontaneous atomic-scale magnetic skyrmion lattice in two dimensions Nat. Phys. 7 713